# Journal Pre-proof


Arsenate removal from aqueous solution by montmorillonite and organo-montmorillonite magnetic materials

Facundo Barraqué, María L. Montes, Mariela A. Fernández, Roberto Candal, Rosa M. Torres Sánchez, Jose L. Marco Brown

PII: S0013-9351(20)31144-0

DOI: https://doi.org/10.1016/j.envres.2020.110247

Reference: YENRS 110247

To appear in: *Environmental Research*

Received Date: 18 April 2020

Revised Date: 10 September 2020

Accepted Date: 16 September 2020

Please cite this article as: Barraqué, F., Montes, M.L., Fernández, M.A., Candal, R., Torres Sánchez, R.M., Marco Brown, J.L., Arsenate removal from aqueous solution by montmorillonite and organo-montmorillonite magnetic materials, *Environmental Research*, https://doi.org/10.1016/j.envres.2020.110247.

Credit Author Statement

Facundo Barraqué: Conceptualization, Methodology, Formal analysis, Investigation, Writing - Original Draft, Writing - Review & Editing, Visualization
María L. Montes: Resources, Writing - Original Draft, Writing - Review & Editing
Mariela A. Fernández: Resources, Writing - Review & Editing
Roberto Candal: Resources, Writing - Review & Editing, Supervision, Funding acquisition
Rosa M. Torres Sánchez: Resources, Writing - Review & Editing, Supervision, Project administration, Funding acquisition
Jose L. Marco Brown: Conceptualization, Methodology, Formal analysis, Validation, Investigation, Resources, Writing - Original Draft, Writing - Review & Editing, Visualization, Supervision, Project administration, Funding acquisition

# Arsenate removal from aqueous solution by montmorillonite and organo-montmorillonite magnetic materials

Facundo Barraqué[a], María L. Montes[b], Mariela A. Fernández[a], Roberto Candal[c], Rosa M. Torres Sánchez[a], Jose L. Marco Brown[c,*]

[a] CETMIC, CICPBA, CONICET CCT-La Plata, Camino Centenario y 506, (B1897ZCA), M. B. Gonnet, Argentina.
[b] IFLP, Instituto de Física La Plata - CONICET CCT-La Plata, Departamento de Física, Facultad de Ciencias Exactas, Universidad Nacional de La Plata, La Plata, Argentina.
[c] Instituto de Investigación e Ingeniería Ambiental IIIA, Universidad Nacional de San Martín, CONICET, UNSAM, Av. 25 de Mayo y Francia, San Martín, Buenos Aires, Argentina.

*Corresponding author. Jose L. Marco Brown

Keywords
Montmorillonite, organo-montmorillonite, magnetite-clay systems, As adsorption, surface complexes.

**Abstract**

Magnetic-clay (MtMag) and magnetic-organoclay (O100MtMag) nanocomposites were synthesized, characterized and evaluated for arsenic adsorption.
Batch arsenic adsorption experiments were performed varying pH conditions and initial As(V) concentration, while successive adsorption cycles were made in order to evaluate the materials reuse. The highest As(V) removal efficiency (9 ± 1 mg $g^{-1}$ and 7.8 ± 0.8 mg $g^{-1}$ for MtMag and O100MtMag, respectively) was found at pH 4.0, decreasing at neutral and alkaline conditions. From As(V) adsorption isotherm, two adsorption processes or two different surface sites were distinguished.
Nanocomposites resulted composed by montmorillonite or organo-montmorillonite and magnetite as the principal iron oxide, with saturation magnetization of 8.5 ± 0.5 $Am^2$ $Kg^{-1}$ (MtMag) and 20.3 ± 0.5 $Am^2$ $Kg^{-1}$ (O100MtMag). Thus, both materials could be separated and recovered from aqueous solutions using external magnetic fields. Both materials allowed achieving arsenic concentrations lower than the World Health Organization (WHO) recommended concentration limit after two consecutive adsorption cycles (2.25 and 4.5 μg $L^{-1}$ for MtMag and O100MtMag, respectively).

## 1. Introduction

The presence of heavy metals and some metalloids in water bodies is still a technological and scientific challenge. In general, the metals elements are wasted from several industries such as tanneries, metallurgic and smelting. In addition, municipal waste, mines residues and fertilizers have a high content of heavy metals which became a local pollution problem (Uddin, 2017).

Particularly, arsenic is a metalloid element found in groundwater mainly due to its release from natural processes such as volcanic phenomena, geochemical reactions and rock disintegration. Also, to a lesser extent, it appears in water bodies through the combustion of fossil fuels and the use of arsenical pesticides. It can be detected in a wide range of concentrations around the world and the limit recommended by the World Health Organization (WHO) is 10 $\mu g\ L^{-1}$. Globally, around 120 countries are affected by the As presence in groundwater. The most impacted countries are Bangladesh, India, Myanmar, Vietnam, Taiwan, and Argentina (Calatayud et al., 2019; Litter et al., 2019).

Arsenic is found in four major oxidation states i.e. -3, 0, +3 and +5. Arsenite ($As^{3+}$) and arsenate ($As^{5+}$) are commonly isolated forms of arsenic in water. As(III) and As(V) species are found in water either as oxy-ions or organic and inorganic molecules. At moderate or high redox potential, pentavalent oxyanions such as $H_2AsO^{4-}$, $HAsO_4^{-2}$ and $AsO_4^{-3}$ are stable while at low redox potential, the stable specie are trivalent oxyanions such as $H_2AsO_3^-$. Various forms of oxyanions, in water, are the result of deprotonation of arsenic ($H_3AsO_4$) or arsenious acid ($H_3AsO_3$) under different redox conditions (Bentahar et al., 2016; Siddiqui et al., 2019). The presence of this pollutant in drinking water can cause important health damage. The long exposition at low As concentration is related with the development of dermal disorders, cancer and diabetes (Iriel et al., 2019) while the short exposure to high As concentration could be lethal (Liu et al., 2015).

Due to the above mentioned, the As removal from water bodies generates an important concern (He et al., 2018; Luong et al., 2018; Niazi et al., 2018; Wu et al., 2018) in order to improve the life quality of people. The physical adsorption process is indicated as efficient, easy to operate and cost-effective to remove polluting substances from water reservoirs. Clay minerals are used worldwide as adsorbent materials of a wide range of pollutants, including heavy metals, organic compounds and dyes, among others, due to its non-toxic nature, low-cost and abundant availability (Uddin, 2017). Particularly, montmorillonite (Mt) clay has a relatively high specific surface area (Michot and Villiéras, 2006) and cation exchange capacity giving them a large potential for ion exchange. While the negative electric charges of clay surfaces are an advantage for the cationic metals retention, it is a drawback to eliminate the inorganic oxyanions such as those formed by arsenic.

Organoclays has attracted interest as a potential adsorbent for arsenic removal (Jin et al., 2012). The presence of functional groups such as hydroxyl, carboxyl and epoxy promote the adsorption of arsenic on the surface of clays. Previous experiments (Barraqué et al., 2018; Bianchi et al., 2013; Jaworski et al., 2019) have revealed that quaternary ammoniums compounds (QAC) loading at values higher than the CEC, modify the Mt surface electrical charge from negative to positive, allowing them to be used to remove inorganic oxyanions.

The use of raw clays as adsorbent materials produces self-agglomeration and difficulty in post-treatment separation of the nanoparticles (Mukhopadhyay et al., 2017). Therefore, the problem related to the separation of contaminated adsorbent from treated water remains.

Iron oxides or different solids coated by them had been used to adsorb negatively charged pollutants, as As (V)/(III), taking advantage of the iron oxide positive surface charge which improves the electrostatic interaction with the adsorbate (Chen et al., 2007; Gallegos-Garcia et al., 2012; Thirunavukkarasu et al., 2003; Zhang et al., 2004). Nevertheless, still remains the problem related to the separation of the polluted adsorbent from the treated water. In order to surpass this tricky situation, several magnetic adsorbent materials have been developed, including magnetite nanoparticles (Liu et al., 2015), biochar/Fe composite (Zhou et al., 2014) and different magnetic composites (Kumar et al., 2014; Lunge et al., 2014; Montes et al., 2020; Yu et al., 2012). Particularly, efficient removal of arsenate by cetyltrimethylammonium bromide modified magnetic nanoparticles has been attained (Jin et al., 2012).

Based on the removal success of inorganic oxyanions and arsenate attained by organoclays and by magnetic nanoparticles, respectively, magnetic-montmorillonite (MtMag) and magnetic organo-montmorillonite (O100MtMag) were proposed as possible low-cost materials for As(V) removal from aqueous solution. The products characterization before and after arsenic adsorption mainly performed by X-ray diffraction (XRD), and zeta potential determination allowed determining surface changes modifications by the adsorption process and also the presence of preferential adsorption sites at the inner or outer surface of the adsorbent, respectively.

## 2. Materials and Methods

### 2.1 Materials and chemicals

The used raw montmorillonite (Mt) was a commercial Argentine Bentonite provided by Castiglioni Pes and Co. from *Río Negro* Province, Argentina. The obtained structural formula through chemical analysis was $[(Si_{3.89}\ Al_{0.11})(Al_{1.43}\ Fe_{0.26}\ Mg_{0.30})]Na_{0.30}Ca_{0.09}K_{0.01}$, while the isoelectric point and the specific surface area were 2.7 and 34 $m^2\ g^{-1}$, respectively (Magnoli et al., 2008). The clay cation exchange capacity (CEC) determined by the Cu-triethylenetetramine method was 0.825 mmol $g^{-1}$ (Gamba et al., 2015).

Magnetic compounds were synthesized using $KNO_3$, KOH (99 % purity) purchased from Biopack and $FeSO_4.7H_2O$ (analytical grade) obtained from Cicarelli Lab.

Surfactant hexadecyltrimethylammonium bromide (HDTMABr) (≥97%) was provided by Fluka (Buchs, Switzerland).

A stock As(V) solution of 1000 mg $L^{-1}$ was prepared dissolving $Na_3AsO_4.7H_2O$ (Biopack analytical grade) in milliQ water (MilliporeGmbH). The working solutions were prepared by dilution to obtain As(V) concentrations ranging from 0.1 to 25.0 mg $L^{-1}$, which is the range documented for As(V) concentration in groundwater in Latin America (Bundschuh et al., 2012; Litter et al., 2019). For this purpose, along all this work, As(V) will be named as As.

### 2.2 Adsorbents material synthesis

The raw montmorillonite was exchanged with $HDTMA^+$ using the procedure described previously (Gamba et al., 2015). Briefly, 4.5 g of HDTMABr, equivalent to 100 % CEC value of Mt, were dissolved in 1 L of distilled water. Then, 15 g of Mt were slowly added and stirred (400 rpm) during 24 h. The product was washed with distilled water to free them of bromide anions (tested by $AgNO_3$). Finally, the solid was lyophilized, milled, labeled as O100Mt and adequately stored into the desiccator.

The magnetic samples designated as MtMag and O100MtMag were obtained using Mt or O100Mt samples as base materials, respectively. The synthesis process was carried out following the procedure described by (Bartonkova et al., 2007). Concisely,

25 mL of $FeSO_4.7H_2O$ (0.3 M) was added to an aqueous Mt or O100Mt suspension with a solid/liquid ratio of 2.5 g/425 mL. The suspension was stirred for 2 h and then 25 mL of $KNO_3$ (0.49 M) and 25 ml of KOH (1.25 M) were added and the temperature was raised to 90 °C. The products obtained were decanted, cooled at room temperature and washed with distilled water. The solids were recovered using a permanent magnet, lyophilized, milled and stored into the desiccator.

2.3 Adsorption batch experiments: pH evaluation and adsorption isotherms

Batch experiments were conducted to determine the equilibrium parameters of the As adsorption onto clay magnetic materials. Experiments were conducted at pH 4.0, 6.0 and 8.0, where the As predominant species are $H_2AsO_4^-$ ($H_3AsO_4$, minority species), $H_2AsO_4^-$ ($HAsO_4^{2-}$, minority species) and $HAsO_4^{2-}$ ($H_2AsO_4^-$, minority species), respectively ($pKa_1$: 2.28; $pKa_2$: 6.97 and $pKa_3$: 11.6) (Iriel et al., 2019). Ionic strength was 1.0 mM $KNO_3$ (that corresponds to conductivity of 160 µS, Hanna, HI 255). Equilibrium experiments were performed with arsenic working solutions with concentrations ranging from 0.1 mg $L^{-1}$ to 25.0 mg $L^{-1}$ and a dose of 0.5 g $L^{-1}$ of adsorbent. Dispersions were maintained upon agitation at 25 ºC for 24 h. Solid and liquid phases were separated by centrifugation and filtration (cellulose nitrate membrane, 0.45 µm). Samples were acidified to 0.5% with $HNO_3$ and stored at 4 ºC until the As measurement. Experiments were carried out by duplicate. Unless otherwise indicated, all data shown are the mean values from two replicate experiments. The typical experimental error was less than 5% for all results.

Arsenic concentration in sample solutions was determined by ICP-OES (Perkin Elmer, Optima DV 2000, USA) according to the methodology reported by (Iriel et al., 2019). The materials adsorption coverage Q for As was calculated as:

$$Q = \frac{(C_0 - C_{eq})V}{m} \qquad (1)$$

where $C_0$ and $C_{eq}$ are both arsenic concentration at initial and equilibrium time in the solution (mg $L^{-1}$), respectively, m is the adsorbent material mass (g) and V the volume of the solution (L).

In order to understand the mechanisms involved in adsorption processes, it is useful to analyze the percentage of removal and surface coverage versus the initial concentration of the adsorbate. As removal (%) was estimated as:

$$\text{As removal (\%)} = \frac{(C_0 - C_{eq}) \times 100}{C_0} \qquad (2)$$

Adsorption isotherms are important criteria for optimizing the use of adsorbent materials because they describe the nature of the interaction between the adsorbate and the adsorbent. Thus, the analysis of the experimentally obtained equilibrium data using either theoretical or empirical equations is useful for the practical design and operation of adsorption systems.

The Langmuir isotherm quantitatively describes the growth of a monolayer of molecules on an adsorbent surface as a function of the concentration of the adsorbed material present in the liquid phase. This model generally reveals a decrease in the number of available interaction sites as the concentration of the adsorbate increases. The Langmuir isotherm is represented by the following equation:

$$Q = \frac{Q_{max} K_L C_{eq}}{(1+K_L C_{eq})} \quad (3)$$

where Q is the surface coverage at equilibrium, $Q_{max}$ is the maximum uptake and represents the maximum concentration that can be accumulated on the solid phase, $C_{eq}$ is the adsorbate concentration at equilibrium in the aqueous solution, and $K_L$ is the Langmuir equilibrium constant, which is related to the free energy of the adsorption. The affinity between the adsorbent and the adsorbate is represented by $K_L$ constant. In general, good adsorbents are those presenting a high $Q_{max}$ and a high $K_L$ (Foo and Hameed, 2010).

The Freundlich isotherm is an empirical equation that describes the adsorption on a heterogeneous surface with a non-uniform distribution of heat of adsorption, which means that the surface, where the adsorbed molecules are interacting, is energetically heterogeneous. This equation does not predict any saturation of the adsorbent by the adsorbate, but infinite surface coverage is predicted, which indicates the presence of multilayer adsorption on the surface. This isotherm is represented by Eq. 4.

$$Q = K_F C_{eq}^{1/n} \quad (4)$$

Here, $K_F$ is the Freundlich constant that indicates the adsorption capacity and represents a measure of the surface area of the adsorbent, and 1/n is an irrational fraction that varies between 0.1 and 1 and is a measure of the adsorption intensity.

The fitting goodness was evaluated following the procedure performed by (Manohar et al., 2006) based on equation (5).

$$\Delta Q = 100 \sqrt{\sum \left( \frac{(Qexp - Qcalc/Qexp)^2}{N-1} \right)} \quad (5)$$

where Qexp and Qcalc are the experimental and predicted clay mineral adsorption coverage values for each As concentration and N the number of evaluated initial concentrations.

2.4 Adsorption cycles

In order to evaluate the reusability, chemical stability and adsorption capacity of the adsorbent materials, three successive arsenic adsorption cycles were carried out in batch systems. Each cycle consisted in three steps: (a) adsorbent dispersion upon agitation at 25 ºC for 24 h on 0.5 mg $L^{-1}$ arsenic solution (dose of adsorbent 1.5 g $L^{-1}$), pH 4 and ionic strength of 1.0 mM $KNO_3$, (b) total supernatant removal by centrifugation (and measure of As concentration), (c) lyophilization and weighing of the pellet obtained after centrifugation. At the end of each cycle, a new one started from (a). Experiments were carried out by duplicate. An adsorbent dosage of 1.5 g $L^{-1}$ was used based on the results obtained from the analysis of the arsenic adsorption isotherms. As can be calculated from the adsorption isotherms, the use of a dosage of 0.5 g $L^{-1}$ would lead to the saturation of the adsorbent in a single cycle.

2.5 Characterization of adsorbents and adsorbate/adsorbent systems

The magnetic samples were characterized by thermogravimetry (Tg), total specific surface area (TSSA) measurements, X-ray diffraction (XRD), zeta potential determinations and vibrating sample magnetometer. Total Fe concentration was determined from Mössbauer spectrum.

Thermogravimetric (Tg) studies were conducted using NETZSCH STA 409 PC/PG. Samples of 50 mg were placed in $Al_2O_3$ crucibles and heated from 25 °C to 1000 °C at a scanning rate of 10 °C $min^{-1}$ in air atmosphere with alumina as a reference. This technic allows it to know the thermal behavior of modified and non-modified samples in order to associate structural differences with thermal events.

The total specific surface area (TSSA) was determined by water vapor adsorption at a relative humidity (rh) of 0.47 (Sánchez and Falasca, 1997). This method was used because those described by the IUPAC recommendations ($N_2$ adsorption, etc.), do not apply to swelling clays. The determination of the TSSA by water adsorption, despite varying due to the presence of different cations in the interlayer, indicates the specific surface area value through hydration (Salles et al., 2009).

Partial X-ray diffraction patterns (from 3 to 20º) were collected by using a Philips PW 1710 diffractometer (Cu$K_\alpha$ radiation, 40 kV and 35 mA), with a counting time equal to 10 s/step and a 0.02° (2θ) step size. Oriented samples, obtained at a constant relative humidity of 0.47 for 48 h, were scanned in order to improve the precision of d001 peak value (Pacuła et al., 2006). X ray diffraction patterns result useful in the determination of interlayer space modification through the measured of d001 value from the reflection of the peak corresponding to 001 plane and the difference with dehydrated montmorillonites d001 value (0.97 nm).

Electrophoretic mobilities values were determined using Brookhaven 90Plus/Bi-MAS and automatically transformed in zeta potential values using the Smoluchowski equation. In order to obtain zeta potential vs pH curves, 40 mg of each sample were dispersed in 40 mL of KCl 1 mM, used as inert electrolyte and the suspensions were continuously stirred and the pH was adjusted adding drops of concentrated KOH or HCl. The zeta potential determination allows inferring electrical surfaces charge changes that could be associated with the adsorption of pollutants on the adsorbent external surface.

The total iron and Fe species concentrations, including magnetite, were estimated by the methodology proposed by (Montes et al., 2016) based on Mössbauer Spectra, which were previously reported (Barraqué et al., 2018).

Hysteresis loops were acquired using external magnetic fields between ±1.9 T in a VSM LakeShore 7404. A diamagnetic sample holder with a negligible magnetic response was used as sample support. The magnetic response against an external magnetic field of adsorbent materials could be evaluated by the saturation magnetization (Ms) determination, and its measurement results important to propose these materials as functional adsorbents. This parameter was extracted from the hysteresis loops after considering the paramagnetic contributions.

## 3. Results and discussion

### 3.1 As adsorption tests

The achieved Q values at the three different pH values (4.0, 6.0 and 8.0) for MtMag and O100MtMag samples are presented in Fig. 1 (solid dosage 0.5 g $L^{-1}$, $C_0$ (As) 10 mg $L^{-1}$ and ionic strength 1 mM $KNO_3$), in order to determine the optimal pH condition to carry out the adsorption isotherm and adsorption cycles experiences. Besides, the adsorption capacity of magnetic materials had been compared with that of the raw Mt sample.

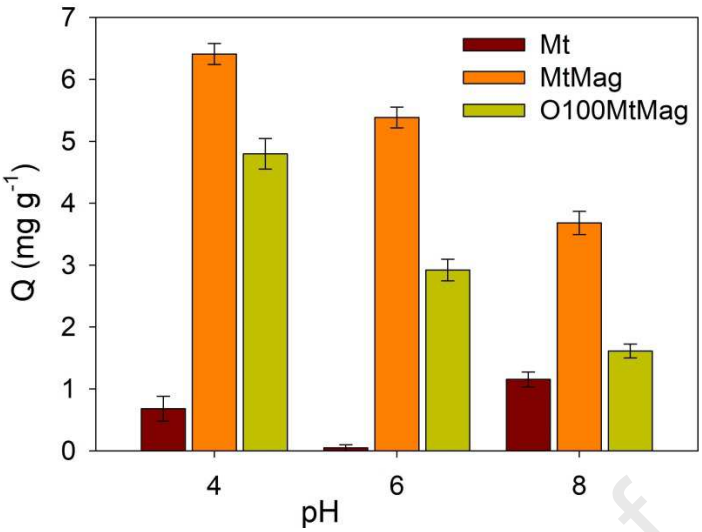


**Fig. 1**. Adsorption of arsenic on indicated samples for the three considered pH values. Solid dosage 0.5 g $L^{-1}$, $C_0$(As) 10 mg $L^{-1}$ and ionic strength 1 mM $KNO_3$.

The Mt adsorption capacity resulted, for the three considered pH values, lower than those determined for magnetic composites, indicating that the proposed clay modifications improved the As adsorption capacity of Mt. In addition, as higher the pH value, the lower the composites adsorption capacity and, therefore, it can be stated that MtMag and O100MtMag exhibited an anionic adsorption profile. Similar results have been reported for the adsorption of picloram (anionic herbicide) on raw clays and montmorillonite modified by Fe oxides (Marco-Brown et al., 2019, 2015, 2014, 2012). It was also reported that As adsorption on goethite and iron modified montmorillonite decreased with the pH increase (Antelo et al., 2005; Iriel et al., 2019). According to these results, foregoing adsorption test were performed at pH 4.0.

Considering that the As species are strongly adsorbed on Fe(III) oxides (Dixit and Hering, 2003), Fe oxides identification and quantification were performed employing Mössbauer spectroscopy. The main identified Fe oxide was magnetite (Barraqué et al., 2018) with total concentrations of 125 ± 10 g $kg^{-1}$ and 168 ± 11 g $kg^{-1}$ for MtMag and O100MtMag samples, respectively. Despite of the higher Fe oxides concentration on O100MtMag, the Q values for this material were significantly lower than for MtMag. This phenomenon may be due to the presence of surfactant in the interlayer space of O100MtMag, hindering the entry of As species (see also Table 2 and XRD analysis discussion).

The As adsorption isotherms on MtMag and O100MtMag at pH 4.0 were depicted in Fig. 2. Adsorption isotherms revealed two successive adsorption processes or two different surface sites involved in the arsenic adsorption. The formation of a monolayer seems to be completed at around 16 mg $L^{-1}$ and 17 mg $L^{-1}$ for MtMag and O100MtMag, respectively. When this concentration was attained, other sites could contribute to the adsorption process. Rearrangement of As adsorbed on MtMag and O100MtMag samples depending on As concentration is proposed below, in order to explain the phenomenon observed.

Experimental data for Ceq lower than 17 mg L-1 were modeled using Freundlich equation (dot lines in Fig. 2) and Langmuir model (solid lines in Fig. 2). It was observed that Freundlich equation represents better the adsorption experimental data than Langmuir model (higher $R^2$ and lower $\Delta Q$). Thus, the fitting results indicated the presence of inhomogeneous adsorption sites. MtMag showed higher adsorption capacity and stronger adsorption intensity than O100MtMag. Fitting results are shown in table 1.

The adsorption maximum capacity achieved for MtMag and O100MtMag resulted lower than that attained by the isolated magnetite reported by (Liu et al., 2015) (Qmax =16 mg $g^{-1}$, 0.01 M NaNO3, 1 g $L^{-1}$, pH=6.5) and comparable with that observed for the magnetite developed for (Darezereshki et al., 2018), (Qmax= 9.72 mg $g^{-1}$ 2 g $L^{-1}$, pH=5.5), and that used by (Shahid et al., 2018), (Qmax = 7.69 mg $g^{-1}$ 1 g $L^{-1}$, pH=6.5). Therefore, despite of the different experimental conditions used in this works, the comparison indicates that clays-magnetic composites are promising materials for As removal, with adsorption capacities comparables to isolated magnetite but without agglomeration and decreasing oxidation probability. Despite of the difference in the experimental conditions for magnetite synthesis and adsorption test the results could indicate that the adsorption performance of non supported magnetite particles would be maintained after its nucleation on clay surfaces."

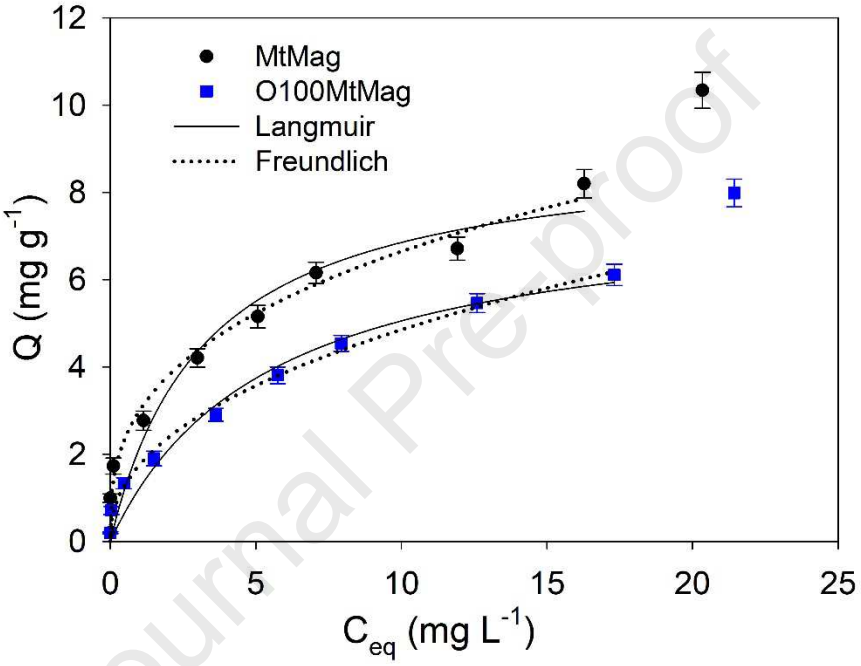


**Fig. 2**. Arsenic adsorption isotherms on (●) MtMag and (■) O100MtMag at solid dosage 0.5 g $L^{-1}$, pH 4 and ionic strength 1 mM $KNO_3$. Solid and dotted lines represent the fitting by Langmuir and Freundlich equations, respectively.

Table 1. Langmuir parameters for As adsorption on MtMag and O100MtMag at solid dosage 0.5 g $L^{-1}$, pH 4 and ionic strength 1 mM $KNO_3$.

| Model | Parameter | MtMag | O100MtMag |
|---|---|---|---|
| Langmuir | $Q_{max}$ (mg $g^{-1}$) | 9±1 | 7.8±0.8 |
| | $K_L$ (L $mg^{-1}$) | 0.3±0.1 | 0.18±0.06 |
| | $R^2$ | 0.935 | 0.968 |
| | ΔQ (%) | 58 | 52 |
| Freundlich | $K_F$ ($L^{1/n}$ $mg^{1-1/n}$ $g^{-1}$) | 3.0±0.2 | 1.75±0.09 |
| | 1/n | 0.35±0.03 | 0.44±0.02 |
| | $R^2$ | 0.982 | 0.994 |
| | ΔQ (%) | 44 | 16 |

In Figure 3, the surface coverage, Q, and the % of arsenic removal are shown as a function of the initial concentration of As. Two distinct areas were indicated: (a) a first zone corresponding to initial concentrations of arsenic up to 20 mg $L^{-1}$ and (b) a second

zone corresponding to $C_0$ of arsenic > 20 mg $L^{-1}$. In the (a) zone, a significant decrease in % removal occurred while the sites available for the adsorption of As were occupied, reaching to an adsorption *plateau*. In the (b) zone, an increase in the surface coverage is observed, while the percentage of arsenic removal remains constant around 20%. This behavior was attributed to a rearrangement of the $H_2AsO_4^-$ molecules adsorbed, as discuses in zeta potential analysis. Both materials presented % removal around 100% for $C_0$ values of 0.1 mg $L^{-1}$ and a % removal greater than 90% for $C_0$ values of 0.5 mg $L^{-1}$. This result is important due to the arsenic concentration range in natural waters in Argentina and Latin America (Bundschuh et al., 2012; Litter et al., 2019).

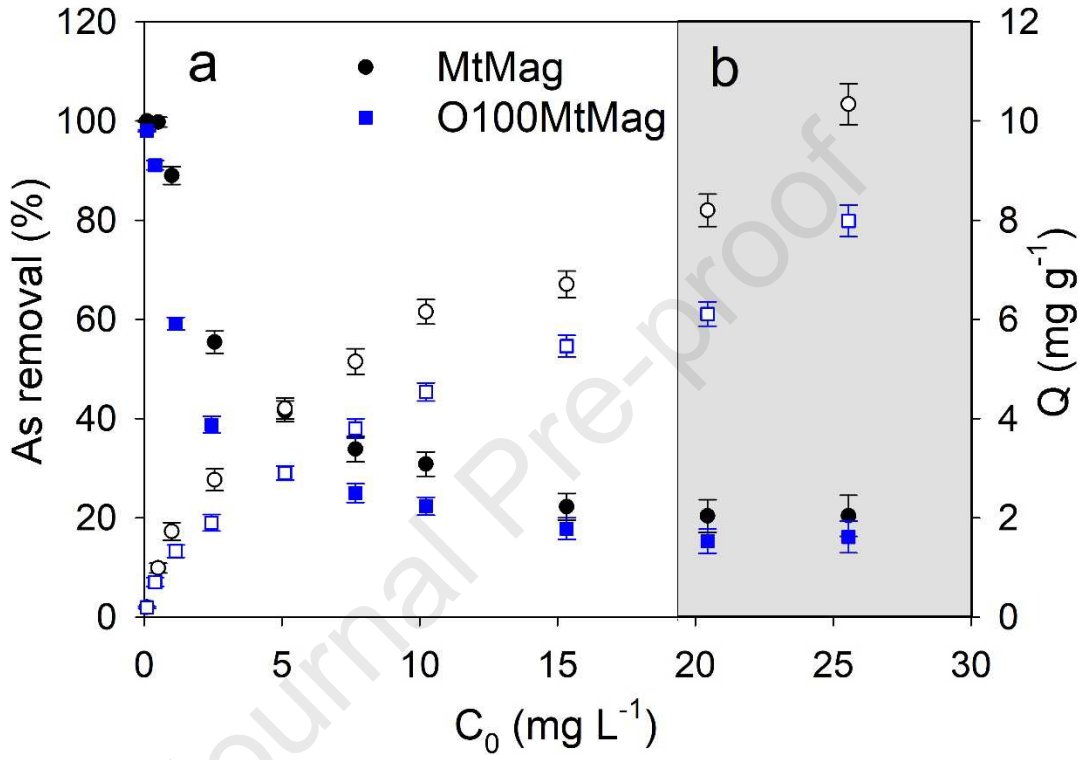


**Fig. 3**. Removal of arsenic by MtMag and O100MtMag samples. Surface coverage, Q (right-axis, empty symbols) and % arsenic removal (left-axis, full symbols), in function of the initial concentration of arsenic. There are two zones (a and b) differentiated by the trends observed for surface coverage and % removal. (Solid dosage 0.5 g $L^{-1}$, pH 4 and ionic strength 1 mM $KNO_3$).

In order to evaluate the capacity of the studied materials to be reused as arsenic adsorbents and consequently, their technological applicability, successive As adsorption cycles were performed. Initial As concentration was 0.5 mg $L^{-1}$, considering the As concentrations commonly found in ground or fresh water in Argentina and Latin America (Bundschuh et al., 2012; Litter et al., 2019). In Figure 4 A and B were indicated the arsenic remainder concentration and the arsenic removal (%) determined after each adsorption cycle, respectively. As can be seen, in the first two cycles, almost completely arsenic removal was achieved for both materials and the arsenic concentration in the supernatant was under the WHO recommended limit. After two cycles, the arsenic removal decline to 70-80% and the arsenic concentration in the supernatant was higher than the WHO recommended limit. This effect is caused by a partial occupancy of surface sites of the adsorbents by As. In order to increase the reusing life of the materials, an increase of the adsorbent dosage should be studied.

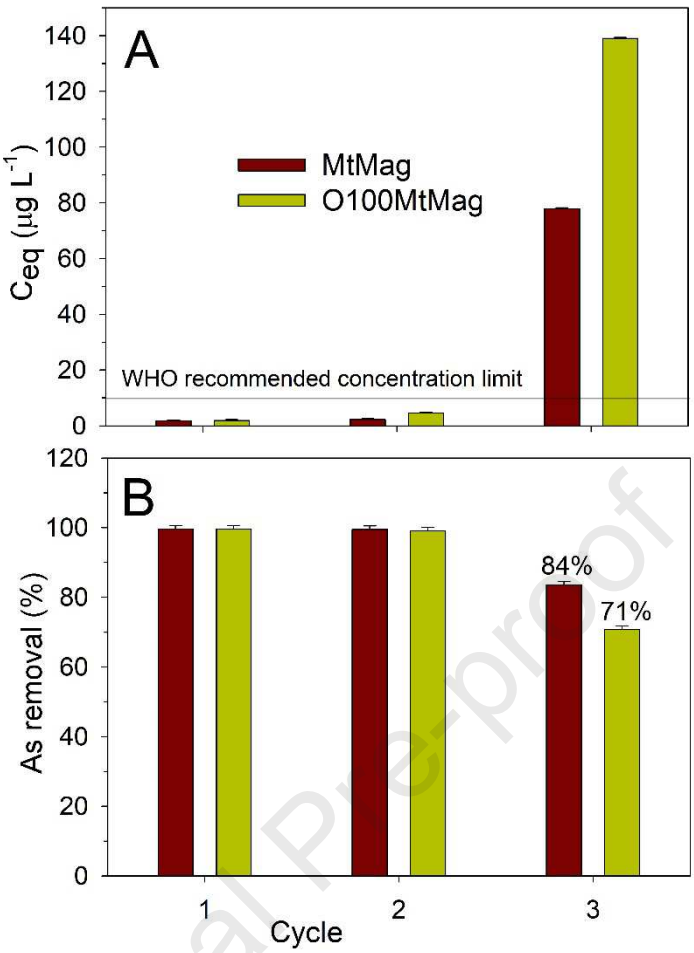


**Fig. 4**. A) Arsenic concentration in supernatant ($Ce_q$) and B) As removal (%), after each adsorption cycle. $C_0$ (As) 0.5 mg $L^{-1}$ (each cycle), solid dosage 1.5 g $L^{-1}$, pH 4 and ionic strength 1 mM $KNO_3$

### 3.2 Materials Characterization

The thermogravimetric curves for Mt, MtMag, O100Mt and O100MtMag samples are shown in Figure 5 A and B. Three zones can be identified, according to the process that occurs in each sample during the assay. The first process, extended up to 100 °C approximately, corresponds to water desorption. In the second range (200 °C - 550 °C) the organic matter is combusted (Gamba et al., 2015), as observed for O100Mt and O100MtMag samples). Finally, at the third zone (550 °C to 700 °C), the dehydroxylation of montmorillonite structure occurs (Wolters and Emmerich, 2007).

Mt sample exhibited a major mass loss than MtMag sample in the first range (Fig. 5 A), due to changes in the nature of the interlayer cations (exchange of sodium by potassium) occurred during the magnetic composite synthesis, (Barraqué et al., 2018) with the consequent loss of hydration water (Liu and Lu, 2006). In addition, a low gain of mass cannot be discarded due to the oxidation of magnetite around these temperatures.

The second range did not show any mass loss because of the absence of organic content. Finally, the last process that starts at 550 °C corresponds to the dehydroxylation of montmorillonite structure. Mt and MtMag samples showed a similar mass loss in this range.

Figure 5 B presents O100Mt and O100MtMag thermal behaviors. During the first step, the sample O100MtMag did not show mass loss (dark cyan solid line). The low

content of water in this sample agrees with the total inner surface modification at the first place by the surfactant load and then by the possibility of potassium and iron ions entrance during magnetic composite synthesis. Besides, the magnetite oxidation could contribute to a low gain of mass. The O100Mt sample presented a lower mass loss than montmorillonite, according to the hydrophobic character of its structure. Besides, an important mass loss was observed in the second zone for both samples, which indicates the surfactant combustion. This mass loss was higher for O100Mt than O100MtMag sample, probably due to the surfactant leaching during the magnetization process. The dehydroxylation process is mixed with the combustion of residual carbon of surfactant in both samples, being the percentage of mass loss slightly higher for O100Mt than O100MtMag sample.

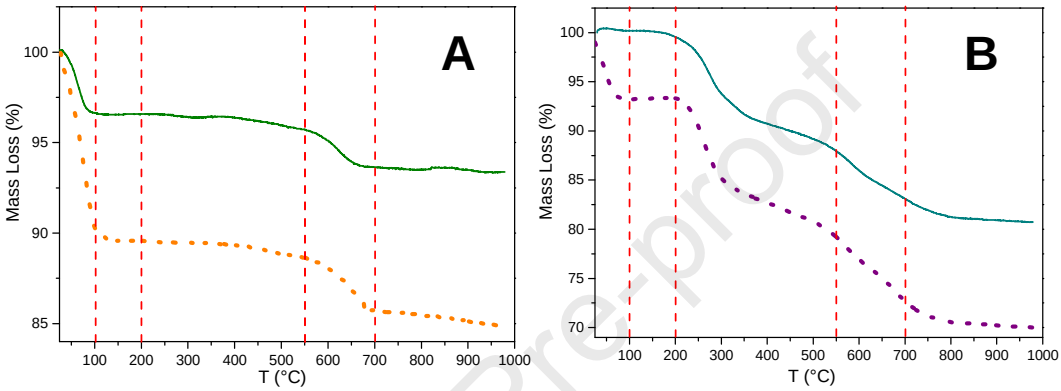


**Fig. 5**. Thermogravimetric analysis for: A) Mt (orange dot line), MtMag (green solid line) and B) O100Mt (purple dot line), O100MtMag (dark cyan solid line). Red lines pretend to separate the process that occurs at different temperature intervals.

The O100MtMag sample has a lower TSSA than MtMag sample, being 14 ± 5 $m^2 g^{-1}$ and 63 ± 5 $m^2 g^{-1}$, respectively. This fact is according to the presence of surfactant at the interlayer space, which has replaced $Na^+$ ions, recognizable water adsorbent. However, the MtMag sample shows an important decrease in the TSSA value respect to that of the Mt sample (164 ± 6 $m^2.g^{-1}$) related to an effect that combine the exchange of sodium ions by potassium ions in the interlayer space during the magnetic composite synthesis and the occupation of Mt surface sites for magnetite particles.

Compositional characterization for the magnetic samples MtMag and O100MtMag were previously performed (Barraqué et al., 2020, 2018). Table 2 presents iron, magnetite, and $HDTMA^+$ content for indicated samples.

Table 2. Iron, Magnetite and $HDTMA^+$ content for the indicated samples.

| Sample | Iron content (g/kg) | Magnetite content (g/kg) | $HDTMA^+$ content (Actual CEC %) |
|---|---|---|---|
| MtMag | 185 ±10 | 120 ±10 | - |
| O100MtMag | 230 ±11 | 152 ±15 | 66 |

Diffraction patterns of oriented samples were presented in Figure 6. The d001 values for MtMag and Mt were quite similar, but the peak had a significant loss of intensity (Fig 6 A and B), assigned to cation exchanges in the interlayer space during the

synthesis of magnetic nanoparticles (Barraqué et al., 2018). In the case of O100MtMag the d001 value was 1.9 nm, assigned to the presence of a pseudotrilayer $HDTMA^+$ arrangement into the Mt gallery (He et al., 2006).

The d001 reflection peak of Mt sample was fitted using two Voight functions (Barraqué et al., 2018). The d001 values achieved were 1.26 and 1.43 nm corresponding to the sodium and calcium presence on montmorillonite interlayer space, respectively, with an area percentage of 70% and 30% for each one.

The sample MtMag did not show any change respect to the d001 value however showed an intensity loss and widening. This behavior was assigned previously to the interlayer cations loss and exchange during the synthesis process of the magnetic component (Barraqué et al., 2018) modifying the area values to 89% for sodium or potassium and to 11% for calcium component of MtMag sample.

The interlayer spaces of Mt and MtMag samples were modified after $H_2AsO_4^-$ adsorption ($C_0$ 10 mg $L^{-1}$, pH 4) (Fig. 6 A and B, respectively). The peaks corresponding to the 001 plane of Mt and MtMag samples after As ($C_0$ 10 mg $L^{-1}$) adsorption were also fitted by two Voight function, due to the clear peak asymmetry (Fig S1). The d001 determined values were similar to that of Mt and MtMag samples without As (1.3 nm and 1.5 nm) but the peak corresponding to 1.5 nm showed a relative area increase until 74% and 61% for Mt and MtMag respectively after As adsorption. This fact allows not neglecting the entry of some species or complexes of As in the interlayer space of both samples. Changes in d001 values achieved could be attributed to $H^+$ entrance in the interlayer space through cation exchange with $Na^+$, which would explain the changes into the Mt gallery. This can be explained by taking into account the lyotropic series or the relative strength of adsorption showed by (Havlin, 2013) $Al^{3+}>H^+>Ca^{2+}>Mg^{2+}>K^+>NH_4^+>Na^+$. According to this, the interaction of protons with the permanent sites charge of clay can be expressed as a cation exchange reaction (Eq. 6):

$$H^+ + NaX \leftrightarrow HX + Na^+ \quad (6)$$

and $Na^+$ ions can be removed by $H^+$ in the pH range of 4-6 with a favorable thermodynamic constant for Na/H exchange indicating a strong affinity of $Na^+$ sites for protons (Tombacz and Szekeres, 2004; Wanner et al., 1994). This fact is in agreement with the results found for (Bourg et al., 2007; Marshall and Krinbill, 1942; Marshall and Bergman, 2002), and (Fletcher and Sposito, 1989).

Nevertheless, the entrance of $H_2AsO_4^-$ in the interlayer space could not be discarded. There were previously stated that anions may enter into the interlayer space of montmorillonites (Damonte et al., 2007; Marco-Brown et al., 2015). Even more, these studies revealed that glyphosate and picloram, two negatively-charged molecules, interact with the negatively charged external and internal surface of montmorillonite through the formation of inner-sphere complexes.

The O100MtMag sample has not shown changes on d001 value after As adsorption (Fig. 6 C), probably because of O100MtMag present a relatively high value (1.9 nm) before adsorption due to the surfactant presence and therefore the entrance of $H_2ASO_4^-$ cannot be revealed by this technic.

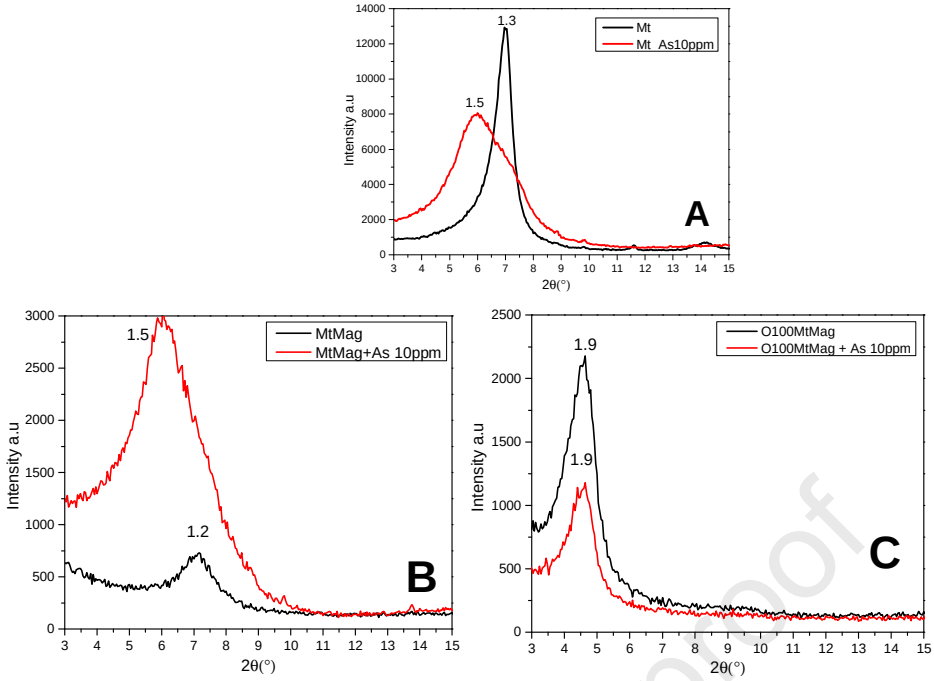


**Fig. 6**. Partial diffraction patterns of indicated oriented samples: A) Mt before and after As adsorption, B) MtMag before and after As adsorption and C) O100MtMag before and after As adsorption. Basal spacing values are expressed in nm.

The zeta potential vs pH curves for Mt, MtMag, and O100MtMag samples before and after arsenic adsorption ($C_0$ 10 mg $L^{-1}$ and $C_0$ 25 mg $L^{-1}$) were displayed in Figure 7. The curves for Mt, MtMag and O100MtMag materials were previously determined and analyzed (Barraqué et al., 2018). Differences in zeta potential values between samples could be explained by the formation of surface complexes between As species and external surface sites of composites. In general, samples after arsenic adsorption resulted less negative than the starting materials except for O100MtMag sample. An extensive interpretation is addressed below.

The sites available for complexes formation at Mt external surface are aluminol groups and iron groups located at edges. In the case of magnetic composites, the sites available for complexes formation at its external surface are mainly iron surface sites of iron particles and aluminol groups.

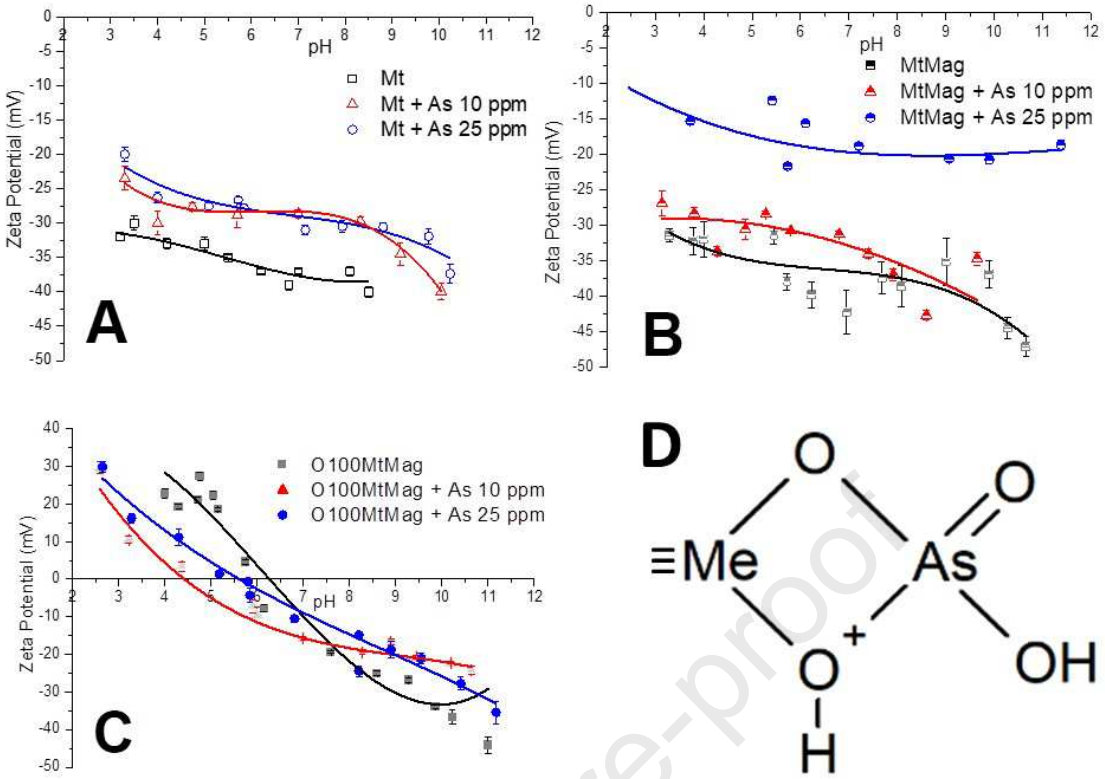


**Fig. 7**. Zeta potential versus pH curves for: A) Mt, B) MtMag, C) O100MtMag, and As adsorbed products, respectively. D) BM complex. ≡Me is referred to iron or aluminol groups in solid surface.

As was indicated before, the predominant arsenic species in the solution is pH-dependent. Moreover, it was recently reported that arsenic adsorption onto nano goethite led to the formation of five different kinds of surface complexes (Han and Ro, 2018). Depending on pH and arsenic concentration, the complexes display different configurations: monodentate mononuclear complex (MM), monodentate binuclear complex (MB), bidentate mononuclear complex (BM), bidentate binuclear complex (BB) and tridentate binuclear complex (TB).

The results obtained from zeta potential studies for Mt samples in this work indicated that different initial concentrations of As led to a similar zeta potential values. This could be indicating similar surface charge behavior after both arsenic concentrations adsorbed.

On the Mt surface, the low amount of iron binding sites and the presence of aluminol (low affinity binding sites) led to the saturation of the adsorbent even at low arsenic initial concentrations. Due to the low As adsorption capacity of montmorillonite, As surface complexes have not been studied before as far as we concern. Nevertheless, the complexes between anions and aluminol surface sites have been extensively studied (He et al., 1997; Marco-Brown et al., 2017) (and references therein) and it has been stated that adsorption of anions on clays might occur on the iron atoms located in edges of the mineral and aluminol groups located at the interlayer/inner and external surface.

Additionally, the zeta potential values of Mt loaded with arsenic were less negative (or more positive) than the values of Mt sample (Fig. 7A). This is indicative of the release of hydroxyl groups followed by a BM, and/or MM and MB complexes formation by coordination of $H_2AsO_4^-$ specie as indicated by equations (7), (8) and (9),

and then the residual electric charge is more positive (Marco-Brown et al., 2012). The interactions between $H_2AsO_4^-$ specie and active surface sites through the formation of BM complexes (Fig. 7D) in equation (8) occurs through the formation of bridge complex and the release of one hydroxyl group, remaining a partial positive charge over arsenate molecule. In equations 7-13, ≡Me is referred to iron or aluminol groups.

$$\equiv MeOH + H_2AsO_4^- \leftrightarrow \equiv MeOAsO_3H_2 \text{ (MM complex)} + OH^- \quad (7)$$

$$\equiv MeOH + H_2AsO_4^- \leftrightarrow \equiv MeO(OH)AsO_2H^+ \text{ (BM complex)} + OH^- \quad (8)$$

$$\equiv Me_2OH + H_2AsO_4^- \leftrightarrow \equiv Me_2OAsO_3H_2 \text{ (MB complex)} + OH^- \quad (9)$$

The MtMag sample exposed to 10 mg $L^{-1}$ of initial arsenic concentration had shown zeta potential values close (but a little more positive) to that of MtMag sample without the pollutant exposition (around -35 mV) in all range of pH studied (Fig. 7B). The same sample in contact with an initial arsenic concentration of 25 mg $L^{-1}$ had shown a considerable change to less negatives values of zeta potential (around -15 mV). At low arsenic concentration (10 mg $L^{-1}$), there are more surface sites available for arsenic adsorption, suggesting the release of hydroxyl groups followed by a mainly bidentate (BB) and tridentate (TB) (and BM, in less extension) complex formation as indicated in equations (8), (10) an (11). Then, the residual charge was slightly more positive, leading to neglectable changes of zeta potential values with regards to that of MtMag (without As). At initial arsenic concentration of 25 mg $L^{-1}$, arsenic complexes are rearranged in order to allow a major adsorption coverage forming BM complex indicated in equation (8).

$$\equiv (MeOH)_2 + H_2AsO_4^- \leftrightarrow \equiv (MeO)_2AsO_2H \text{ (BB complex)} + H_2O + OH^- \quad (10)$$

$$\equiv Me_2(OH)_3 + H_2AsO_4^- \leftrightarrow \equiv Me_2O_3AsO \text{ (TB complex)} + 2H_2O + OH^- \quad (11)$$

As was indicated above, an increase of arsenic adsorption beyond an As concentration of 16-17 mg $L^{-1}$ was found (Figure 2) and this might be related to two different adsorption processes or to two different surface sites involved in As adsorption. These results support the rearrangement of arsenate species at the surface of iron oxides, suggested before to explain the changes in zeta potential curves when arsenic initial concentration was increased (Fig 7 B).

For O100MtMag sample (Fig. 7C) the behavior of the surface charges was attributed to a mixing behavior of magnetite and O100Mt components. It revealed an isoelectric point (IEP) around pH 6.0, close to that of magnetite ($IEP_{pH}$ = 6.7), due to higher magnetite content respect to MtMag sample (Barraqué et al., 2018). Afterward arsenic adsorption, the zeta potential values had slightly turned to less positive below to pH 7.0 and faintly more positive above pH 7.0 at both evaluated initial arsenic concentration, compared with O100MTMag curve (Fig. 7C).

Underneath pH 7.0, the less positive values of zeta potential curve of the sample with arsenic initial concentration of 10 mg $L^{-1}$ compared to sample without arsenic, could be explained by the formation of TB complex between $H_2AsO_4^-$ specie and partial protonated iron/aluminum surface sites according to equation (12). The release of a hydronium ion as indicated, conduce a residual charge less positive.

$$\equiv MeOH_2^+ + \equiv MeOH + H_2AsO_4^- \leftrightarrow \equiv Me_2O_3AsO \text{ (TB complex)} + H_2O + H_3O^+ \quad (12)$$

Below pH 7.0, for sample equilibrated with 25 mg $L^{-1}$ of As, a rearrangement of a fraction of arsenic adsorbed occurs, conducting to the formation of MM complexes as indicated in equation (13). The release of $H_2O$ molecules produces less negative values of zeta potential compared to sample with 10 mg $L^{-1}$ of arsenic. The rearrangement of arsenic adsorbed when its initial concentration increase, proposed by zeta potential results, are in agreement with arsenic adsorption isotherms (Figure 2).

$$\equiv MeOH_2^+ + H_2AsO_4^- \leftrightarrow \equiv MeOAsO_3H_2 \text{ (MM complex)} + H_2O \quad (13)$$

Above pH 7.0, at both evaluated initial arsenic concentration, similar values of zeta potential were obtained. These results could be indicating the formation of a mixture of complexes MM, BM, BB and TB (see equations (7), (8), (10) and (11)). Along with the evidence generated by XRD results and the oxide content, this behavior could be indicating that the preference sites adsorption on O100MtMag was the composite external surface but arsenic species interlayer entrance cannot be discarded.

Hysteresis loops of MtMag and O100MtMag were measured in previous work which allowed to calculate magnetic parameters including the saturation magnetization (Ms), the most technologically relevant magnetic parameter, due to as higher the Ms easier to manipulate the material by an external magnetic field. Although MtMag and O100MtMag showed a magnetic response, the O100MtMag sample presented the highest Ms value (Table 3).

The saturation magnetization values of both magnetic samples did not show significant differences after 10 mg $L^{-1}$ and 25 mg $L^{-1}$ arsenic exposition. Besides, Ms values did not change after two arsenic adsorption cycles, indicating that the magnetic response is not affected by the arsenic adsorption procedure (Table 3). This is, from the technological point of view, a promising result, due to the capacity of manipulating the composites by external magnetic fields is not being degraded.

Table 3. Saturation magnetization (Ms) expressed in $Am^2\ kg^{-1}$ for indicated samples.

| Sample | Raw Material | Adsorbent + As 10 mg $L^{-1}$ | Adsorbent + As 25 mg $L^{-1}$ | Adsorbent after 3 cycles |
|---|---|---|---|---|
| MtMag | 8.5 ± 0.5 | 8.7 ± 0.5 | 8.1 ± 0.5 | 8.9 ± 0.5 |
| O100MtMag | 20.3 ± 0.5 | 20.6 ± 0.5 | 20.3 ± 0.5 | 19.8 ± 0.5 |

## 4. Conclusions

Montmorillonite and organic montmorillonite (exchanged by $HDTMA^+$, 100 % Mt CEC) were modified by magnetic material nucleation and used as arsenic adsorption materials. The adsorption isotherms reveal inhomogeneous adsorption sites, supported by changes on the interlayer space and the external surface charge, where the external surface seems to present the preferential sites, however, the interlayer sites cannot be discarded with the aforementioned evidence. The Langmuir fitted model allows calculating a higher maximum capacity of adsorption for MtMag (9±1 mg g-1) than O100MtMag (7.8±0.8 mg g-1). Both adsorbent materials could be successfully used in two successive cycles of As removal in order to achieve arsenic concentrations lower than the limit proposed by WHO.

Considering that O100MtMag presented a suitable capacity of As adsorption and considerably higher Ms value than MtMag, which allows a more efficient indirect manipulation by an external magnetic field, the former is proposed as technologically appropriate arsenic adsorbent material.

**Acknowledgements**

Financial support of Argentine Ministry of Science, ANPCyT- PICT 585/2014, 2386/2014 and PICT 1260/2015 is gratefully acknowledged. M.L.M., M.A.F, J.L.M.B. and R.C. are members of National Council of Scientific and Technological Research (CONICET) and F.B. acknowledged CONICET fellowship.

## References

Antelo, J., Avena, M., Fiol, S., López, R., Arce, F., 2005. Effects of pH and ionic strength on the adsorption of phosphate and arsenate at the goethite–water interface. J. Colloid Interface Sci. 285, 476–486. https://doi.org/10.1016/j.jcis.2004.12.032

Barraqué, F., Montes, L., Fernandez, M., Candal, R., Mercader, R., Torres Sanchez, R., 2020. Synthesis of high-saturation magnetization composites by montmorillonite loading with hexadecyl trimethyl ammonium ions and magnetite nucleation for improved effluent sludge handling and dye removal. Appl. Phys. A.

Barraqué, F., Montes, M.L., Fernández, M.A., Mercader, R.C., Candal, R.J., Torres Sánchez, R.M., 2018. Synthesis and characterization of magnetic-montmorillonite and magnetic-organo-montmorillonite: Surface sites involved on cobalt sorption. J. Magn. Magn. Mater. 466, 376–384.

Bartonkova, H., Mashlan, M., Medrik, I., Jancik, D., Zboril, R., 2007. Magnetically modified bentonite as a possible contrast agent in MRI of gastrointestinal tract. Chem. Pap. 61, 413–416.

Bentahar, Y., Hurel, C., Draoui, K., Khairoun, S., Marmier, N., 2016. Adsorptive properties of Moroccan clays for the removal of arsenic(V) from aqueous solution. Appl. Clay Sci. 119, 385–392. https://doi.org/10.1016/j.clay.2015.11.008

Bianchi, A.E., Fernández, M., Pantanetti, M., Viña, R., Torriani, I., Sánchez, R.M.T., Punte, G., 2013. ODTMA+ and HDTMA+ organo-montmorillonites characterization: New insight by WAXS, SAXS and surface charge. Appl. Clay Sci. 83–84, 280–285. https://doi.org/10.1016/j.clay.2013.08.032

Bourg, I.C., Sposito, G., Bourg, A.C.M., 2007. Modeling the acid–base surface chemistry of montmorillonite. J. Colloid Interface Sci. 312, 297–310. https://doi.org/10.1016/j.jcis.2007.03.062

Bundschuh, J., Litter, M.I., Parvez, F., Román-Ross, G., Nicolli, H.B., Jean, J.-S., Liu, C.-W., López, D., Armienta, M.A., Guilherme, L.R.G., Cuevas, A.G., Cornejo, L., Cumbal, L., Toujaguez, R., 2012. One century of arsenic exposure in Latin America: A review of history and occurrence from 14 countries. Sci. Total Environ., Special Section - Arsenic in Latin America, An Unrevealed Continent: Occurence, Health Effects and Mitigation 429, 2–35. https://doi.org/10.1016/j.scitotenv.2011.06.024

Calatayud, M., Farias, S.S., de Paredes, G.S., Olivera, M., Carreras, N.Á., Giménez, M.C., Devesa, V., Vélez, D., 2019. Arsenic exposure of child populations in Northern Argentina. Sci. Total Environ. 669, 1–6. https://doi.org/10.1016/j.scitotenv.2019.02.415

Chen, W., Parette, R., Zou, J., Cannon, F.S., Dempsey, B.A., 2007. Arsenic removal by iron-modified activated carbon. Water Res. 41, 1851–1858. https://doi.org/10.1016/j.watres.2007.01.052

Damonte, M., Sánchez, R.M.T., dos Santos Afonso, M., 2007. Some aspects of the glyphosate adsorption on montmorillonite and its calcined form. Appl. Clay Sci. 36, 86–94.

Darezereshki, E., khodadadi Darban, A., Abdollahy, M., Jamshidi-Zanjani, A., 2018. Influence of heavy metals on the adsorption of arsenate by magnetite nanoparticles: kinetics and thermodynamic. Environ. Nanotechnol. Monit. Manag. 10, 51–62.

Dixit, S., Hering, J.G., 2003. Comparison of Arsenic(V) and Arsenic(III) Sorption onto Iron Oxide Minerals: Implications for Arsenic Mobility. Environ. Sci. Technol. 37, 4182–4189. https://doi.org/10.1021/es030309t

Fletcher, P., Sposito, G., 1989. The chemical modelling of clay/electrolyte interactions for montmorillonite. Clay Miner. 24, 375–391.

Foo, K.Y., Hameed, B.H., 2010. Insights into the modeling of adsorption isotherm systems. Chem. Eng. J. 156, 2–10.

Gallegos-Garcia, M., Ramírez-Muñiz, K., Song, S., 2012. Arsenic Removal from Water by Adsorption Using Iron Oxide Minerals as Adsorbents: A Review. Miner. Process. Extr. Metall. Rev. 33, 301–315. https://doi.org/10.1080/08827508.2011.584219

Gamba, M., Flores, F.M., Madejová, J., Torres Sánchez, R.M., 2015. Comparison of Imazalil Removal onto Montmorillonite and Nanomontmorillonite and Adsorption Surface Sites Involved: An Approach for Agricultural Wastewater Treatment. Ind. Eng. Chem. Res. 54, 1529–1538. https://doi.org/10.1021/ie5035804

Han, J., Ro, H.-M., 2018. Identification of Bernalite Transformation and Tridentate Arsenate Complex at Nano-goethite under Effects of Drying, pH and Surface Loading. Sci. Rep. 8, 1–10. https://doi.org/10.1038/s41598-018-26808-4

Havlin, J.L., 2013. Fertility, in: Reference Module in Earth Systems and Environmental Sciences. Elsevier, p. B9780124095489050000. https://doi.org/10.1016/B978-0-12-409548-9.05162-9

He, H., Frost, R.L., Bostrom, T., Yuan, P., Duong, L., Yang, D., Xi, Y., Kloprogge, J.T., 2006. Changes in the morphology of organoclays with HDTMA+ surfactant loading. Appl. Clay Sci. 31, 262–271. https://doi.org/10.1016/j.clay.2005.10.011

He, L.M., Zelazny, L.W., Martens, D.C., Baligar, V.C., Ritchey, K.D., 1997. Ionic Strength Effects on Sulfate and Phosphate Adsorption on γ-Alumina and Kaolinite: Triple-Layer Model. Soil Sci. Soc. Am. J. 61, 784–793. https://doi.org/10.2136/sssaj1997.03615995006100030011x

He, R., Peng, Z., Lyu, H., Huang, H., Nan, Q., Tang, J., 2018. Synthesis and characterization of an iron-impregnated biochar for aqueous arsenic removal. Sci. Total Environ. 612, 1177–1186. https://doi.org/10.1016/j.scitotenv.2017.09.016

Iriel, A., Marco-Brown, J.L., Diljkan, M., Trinelli, M.A., dos Santos Afonso, M., Fernández Cirelli, A., 2019. Arsenic Adsorption on Iron-Modified Montmorillonite: Kinetic Equilibrium and Surface Complexes. Environ. Eng. Sci. https://doi.org/10.1089/ees.2019.0220

Jaworski, M.A., Flores, F.M., Fernández, M.A., Casella, M., Torres Sánchez, R.M., 2019. Use of organo-montmorillonite for the nitrate retention in water: influence of alkyl length of loaded surfactants. SN Appl. Sci. 1, 1318. https://doi.org/10.1007/s42452-019-1349-8

Jin, Y., Liu, F., Tong, M., Hou, Y., 2012. Removal of arsenate by cetyltrimethylammonium bromide modified magnetic nanoparticles. J. Hazard. Mater. 227–228, 461–468. https://doi.org/10.1016/j.jhazmat.2012.05.004

Kumar, S., Nair, R.R., Pillai, P.B., Gupta, S.N., Iyengar, M.A.R., Sood, A.K., 2014. Graphene Oxide–MnFe2O4 Magnetic Nanohybrids for Efficient Removal of Lead and Arsenic from Water. ACS Appl. Mater. Interfaces 6, 17426–17436. https://doi.org/10.1021/am504826q

Litter, M.I., Ingallinella, A.M., Olmos, V., Savio, M., Difeo, G., Botto, L., Farfán Torres, E.M., Taylor, S., Frangie, S., Herkovits, J., Schalamuk, I., González, M.J., Berardozzi, E., García Einschlag, F.S., Bhattacharya, P., Ahmad, A., 2019. Arsenic in Argentina: Occurrence, human health, legislation and determination. Sci. Total Environ. 676, 756–766. https://doi.org/10.1016/j.scitotenv.2019.04.262

Liu, C.-H., Chuang, Y.-H., Chen, T.-Y., Tian, Y., Li, H., Wang, M.-K., Zhang, W., 2015. Mechanism of Arsenic Adsorption on Magnetite Nanoparticles from Water: Thermodynamic and Spectroscopic Studies. Environ. Sci. Technol. 49, 7726–7734. https://doi.org/10.1021/acs.est.5b00381

Liu, X.-D., Lu, X.-C., 2006. A Thermodynamic Understanding of Clay-Swelling Inhibition by Potassium Ions. Angew. Chem. Int. Ed. 45, 6300–6303. https://doi.org/10.1002/anie.200601740

Lunge, S., Singh, S., Sinha, A., 2014. Magnetic iron oxide (Fe3O4) nanoparticles from tea waste for arsenic removal. J. Magn. Magn. Mater. 356, 21–31. https://doi.org/10.1016/j.jmmm.2013.12.008

Luong, V.T., Cañas Kurz, E.E., Hellriegel, U., Luu, T.L., Hoinkis, J., Bundschuh, J., 2018. Iron-based subsurface arsenic removal technologies by aeration: A review of the current state and future prospects. Water Res. 133, 110–122. https://doi.org/10.1016/j.watres.2018.01.007

Magnoli, A.P., Tallone, L., Rosa, C.A.R., Dalcero, A.M., Chiacchiera, S.M., Torres Sanchez, R.M., 2008. Commercial bentonites as detoxifier of broiler feed contaminated with aflatoxin. Appl. Clay Sci. 40, 63–71. https://doi.org/10.1016/j.clay.2007.07.007

Manohar, D.M., Noeline, B.F., Anirudhan, T.S., 2006. Adsorption performance of Al-pillared bentonite clay for the removal of cobalt(II) from aqueous phase. Appl. Clay Sci. 31, 194–206. https://doi.org/10.1016/j.clay.2005.08.008

Marco-Brown, J.L., Areco, M.M., Torres Sánchez, R.M., dos Santos Afonso, M., 2014. Adsorption of picloram herbicide on montmorillonite: Kinetic and equilibrium studies. Colloids Surf. Physicochem. Eng. Asp. 449. https://doi.org/10.1016/j.colsurfa.2014.02.038

Marco-Brown, J.L., Barbosa-Lema, C.M., Torres Sánchez, R.M., Mercader, R.C., dos Santos Afonso, M., 2012. Adsorption of picloram herbicide on iron oxide pillared montmorillonite. Appl. Clay Sci. 58, 25–33. https://doi.org/10.1016/j.clay.2012.01.004

Marco-Brown, J.L., Gaigneaux, E.M., Sánchez, R.M.T., Afonso, M. dos S., 2019. Adsorption of picloram on clays nontronite, illite and kaolinite: equilibrium and herbicide-clays surface complexes. J. Environ. Sci. Health Part B 54, 281–289. https://doi.org/10.1080/03601234.2018.1561055

Marco-Brown, J.L., Trinelli, M.A., Gaigneaux, E.M., Torres Sánchez, R.M., dos Santos Afonso, M., 2015. New insights on the structure of the picloram–montmorillonite surface complexes. J. Colloid Interface Sci. 444, 115–122. https://doi.org/10.1016/j.jcis.2014.12.045

Marco-Brown, J.L., Undabeytia, T., Torres Sánchez, R.M., dos Santos Afonso, M., 2017. Slow-release formulations of the herbicide picloram by using Fe–Al pillared montmorillonite. Environ. Sci. Pollut. Res. 24, 10410–10420. https://doi.org/10.1007/s11356-017-8699-9

Marshall, C., Krinbill, C., 1942. The Clays as Colloidal Electrolytes. J. Phys. Chem. 46, 1077–1090.

Marshall, C.E., Bergman, W.E., 2002. The Electrochemical Properties of Mineral Membranes. II. Measurement of Potassium-ion Activities in Colloidal Clays. [WWW Document]. https://doi.org/10.1021/j150415a007

Michot, L.J., Villiéras, F., 2006. Chapter 12.9 Surface Area and Porosity, in: Bergaya, F., Theng, B.K.G., Lagaly, G. (Eds.), Developments in Clay Science, Handbook of Clay Science. Elsevier, pp. 965–978. https://doi.org/10.1016/S1572-4352(05)01035-4

Montes, M.L., Barraqué, F., Bursztyn Fuentes, A.L., Taylor, M.A., Mercader, R.C., Miehé-Brendlé, J., Torres Sánchez, R.M., 2020. Effect of synthetic beidellite structural characteristics on the properties of beidellite/Fe oxides magnetic composites as Sr and Cs adsorbent materials. Mater. Chem. Phys. 245, 122760. https://doi.org/10.1016/j.matchemphys.2020.122760

Montes, M.L., Rivas, P.C., Taylor, M.A., Mercader, R.C., 2016. Approximate total Fe content determined by Mössbauer spectrometry: Application to determine the correlation between gamma-ray-emitter activities and total content of Fe phases in soils of the Province of Buenos Aires, Argentina. J. Environ. Radioact. 162–163, 113–117. https://doi.org/10.1016/j.jenvrad.2016.05.016

Mukhopadhyay, R., Manjaiah, K.M., Datta, S.C., Yadav, R.K., Sarkar, B., 2017. Inorganically modified clay minerals: Preparation, characterization, and arsenic adsorption in contaminated water and soil. Appl. Clay Sci. 147, 1–10. https://doi.org/10.1016/j.clay.2017.07.017

Niazi, N.K., Bibi, I., Shahid, M., Ok, Y.S., Burton, E.D., Wang, H., Shaheen, S.M., Rinklebe, J., Lüttge, A., 2018. Arsenic removal by perilla leaf biochar in aqueous solutions and groundwater: An integrated spectroscopic and microscopic examination. Environ. Pollut. 232, 31–41. https://doi.org/10.1016/j.envpol.2017.09.051

Pacuła, A., Bielańska, E., Gaweł, A., Bahranowski, K., Serwicka, E.M., 2006. Textural effects in powdered montmorillonite induced by freeze-drying and ultrasound pretreatment. Appl. Clay Sci. 32, 64–72. https://doi.org/10.1016/j.clay.2005.10.002

Salles, F., Douillard, J.-M., Denoyel, R., Bildstein, O., Jullien, M., Beurroies, I., Van Damme, H., 2009. Hydration sequence of swelling clays: Evolutions of specific surface area and hydration energy. J. Colloid Interface Sci. 333, 510–522.

Shahid, M.K., Phearom, S., Choi, Y.-G., 2018. Synthesis of magnetite from raw mill scale and its application for arsenate adsorption from contaminated water. Chemosphere 203, 90–95.

Siddiqui, S.I., Naushad, Mu., Chaudhry, S.A., 2019. Promising prospects of nanomaterials for arsenic water remediation: A comprehensive review. Process Saf. Environ. Prot. 126, 60–97. https://doi.org/10.1016/j.psep.2019.03.037

Thirunavukkarasu, O.S., Viraraghavan, T., Subramanian, K.S., 2003. Arsenic Removal from Drinking Water using Iron Oxide-Coated Sand. Water. Air. Soil Pollut. 142, 95–111. https://doi.org/10.1023/A:1022073721853

Tombacz, E., Szekeres, M., 2004. Colloidal behavior of aqueous montmorillonite suspensions: the specific role of pH in the presence of indifferent electrolytes. Appl. Clay Sci. 27, 75–94.

Uddin, M.K., 2017. A review on the adsorption of heavy metals by clay minerals, with special focus on the past decade. Chem. Eng. J. 308, 438–462. https://doi.org/10.1016/j.cej.2016.09.029

Wanner, H., Albinsson, Y., Karnland, O., Wieland, E., Wersin, P., Charlet, L., 1994. The acid/base chemistry of montmorillonite. Radiochim. Acta 66, 157–162.

Wolters, F., Emmerich, K., 2007. Thermal reactions of smectites—Relation of dehydroxylation temperature to octahedral structure. Thermochim. Acta 462, 80–88. https://doi.org/10.1016/j.tca.2007.06.002

Wu, L.-K., Wu, H., Zhang, H.-B., Cao, H.-Z., Hou, G.-Y., Tang, Y.-P., Zheng, G.-Q., 2018. Graphene oxide/CuFe2O4 foam as an efficient absorbent for arsenic removal from water. Chem. Eng. J. 334, 1808–1819. https://doi.org/10.1016/j.cej.2017.11.096

Yu, X., Tong, S., Ge, M., Zuo, J., Cao, C., Song, W., 2012. One-step synthesis of magnetic composites of cellulose@iron oxide nanoparticles for arsenic removal. J. Mater. Chem. A 1, 959–965. https://doi.org/10.1039/C2TA00315E

Zhang, W., Singh, P., Paling, E., Delides, S., 2004. Arsenic removal from contaminated water by natural iron ores. Miner. Eng. 17, 517–524. https://doi.org/10.1016/j.mineng.2003.11.020

Zhou, Y., Gao, B., Zimmerman, A.R., Chen, H., Zhang, M., Cao, X., 2014. Biochar-supported zerovalent iron for removal of various contaminants from aqueous solutions. Bioresour. Technol. 152, 538–542. https://doi.org/10.1016/j.biortech.2013.11.021

- Arsenic adsorption by clays composites involves the formation of several complexes.
- Magnetic composites can be useful to reduce the health risk due to pollutants manipulation.
- Zeta potential measurements are crucial to determine the sites of composite for As adsorption
- Magnetic composites can be used until two times to decrease the As concentration considerably.

**Declaration of interests**

☒ The authors declare that they have no known competing financial interests or personal relationships that could have appeared to influence the work reported in this paper.

☐The authors declare the following financial interests/personal relationships which may be considered as potential competing interests: